ChemComm

COMMUNICATION

View Article Online
View Journal | View Issue

Cite this: *Chem. Commun.*, 2022, **58**, 4524

Received 14th December 2021,
Accepted 7th March 2022

DOI: 10.1039/d1cc06974h

rsc.li/chemcomm

New chiral ECD-Raman spectroscopy of atropisomeric naphthalenediimides†

Ewa Machalska, [ab] Grzegorz Zając, *[bc] Malgorzata Baranska, [ab] Petr Bouř, *[c] Dorota Kaczorek, [d] Robert Kawęcki, *[d] Joanna E. Rode, [e] Krzysztof Lyczko [e] and Jan Cz. Dobrowolski *[e]

In this study, we found that a recently discovered ECD-Raman effect dominated over the natural Raman optical activity in a series of atropisomeric naphthalenediimides, and we investigated the kind of information about the molecular structure that could be obtained from the spectra. The ECD-Raman effect is polarised Raman scattering modulated by electronic circular dichroism. We showed that the spectra significantly depended on the substitution of the solute and/or the change of the solvent. Moreover, the spectra could be well-predicted by the theory, thus providing an interesting tool to monitor the chirality of the binaphthyl compounds.

While polarised Raman measurements and Electronic Circular Dichroism (ECD) spectroscopy have been known for a long time, the ECD-Raman (or eCP-Raman) effect was recognized only recently.[1–3] It can be observed that some chiral species absorb light within the Raman scattering range as an additional component of the signal when Raman optical activity (ROA) is measured.[4,5] The ROA method is a form of chiroptical spectroscopy that is quickly rising in popularity. This method is complementary to Vibrational Circular Dichroism (VCD) in an analogous way to Raman and IR spectroscopies. ROA offers easy measurements in water and in the 800–100 cm^{-1} range, which is difficult to access by VCD. Moreover, ROA enables the possibility to remarkably enhance a signal due to resonance effects. This is why ROA can be successfully applied to study the conformation, absolute configuration, and enantiomeric excess of biomolecules in their native systems.

Until late 2020, the ECD-Raman response to a laser beam was puzzling.[6–8] For example, the response was attributed to resonance ROA (RROA). In fact, the Single Electronic State theory predicted monosignate RROA spectra that were often observed.[9–11] In pre-resonance and in the presence of more electronic states[12–14] or conformers,[15,16] RROA can be bisignate.[17]

However, it was soon clear that the effect could not be explained by RROA alone, as very strong bands of achiral solvent were also seen. The solute bands, which were potentially attributable to RROA, remained weak or even invisible.[2] The sign of the strong bands did not clearly correlate with ECD only.[6–8]

Other mechanisms to which the ECD-Raman effect has been inaccurately attributed include the resonance energy transfer (RET)[18] responsible for a chirality transfer from a chiral solute to an achiral solvent.[6–8] Eventually, Wu *et al.*[1] and then Machalska *et al.*[2] and Li *et al.*[3] showed that the effect was due to the ECD of colour samples combined with circularly polarised (CP) Raman scattering.[19] For the normalised ECD-Raman circular intensity difference (CID) a Beer–Lambert-like formula was derived:[2]

$$\mathrm{CID} = \frac{I_R - I_L}{I_R + I_L} = a_{\mathrm{ECDR}} \cdot c \cdot l \qquad (1)$$

where I_R and I_L are the detected right and left CP light intensities, c is the concentration, and $l = (L + 2L')$, where L is the Raman active pathlength and L' is the ECD-active pathlength,

$$a_{\mathrm{ECDR}} = \frac{\ln 10}{4} \cdot \Delta\varepsilon \cdot \left(\frac{\Delta\varepsilon'}{\Delta\varepsilon} + \mathrm{DOC} \right) \qquad (2)$$

$\Delta\varepsilon = \varepsilon_L - \varepsilon_R$ is the differential absorption coefficient at the incident wavelength (532 nm), and the prime (′) mark refers to each Raman band, for a solvent or a solute. The ln 10 factor was absent in the first derivation,[1] because natural absorption

[a] *Faculty of Chemistry, Jagiellonian University, Gronostajowa 2, 30-387 Cracow, Poland*
[b] *Jagiellonian Centre for Experimental Therapeutics (JCET), Jagiellonian University, Bobrzynskiego 14, 30-348 Cracow, Poland. E-mail: grzesiek.zajac@uj.edu.pl*
[c] *Institute of Organic Chemistry and Biochemistry, Academy of Sciences, Flemingovo náměstí 2, 16610, Prague, Czech Republic. E-mail: bour@uochb.cas.cz*
[d] *Faculty of Science, Siedlce University, 3 Maja Street No. 54, 08-110 Siedlce, Poland. E-mail: robert.kawecki@uph.edu.pl*
[e] *Laboratory for Spectroscopy, Molecular Modeling and Structure Determination, Institute of Nuclear Chemistry and Technology, 16 Dorodna-Street, 03-195 Warsaw, Poland. E-mail: j.dobrowolski@nil.gov.pl*

† Electronic supplementary information (ESI) available: (1) Syntheses and characterization of products; (2) crystallographic data and brief description of interactions present in the crystals; (3) calculations of the substituent effect and visualization of the HOMO and LUMO states; (4) ECD, Raman, ECD-Raman experiments and additional experimental data; (5) study of the origin of the first ECD sign; (6) Raman, ROA, and pre-RROA spectra as well as the ECD-Raman spectra. CCDC 2116384–2116387. For ESI and crystallographic data in CIF or other electronic format see DOI: 10.1039/d1cc06974h

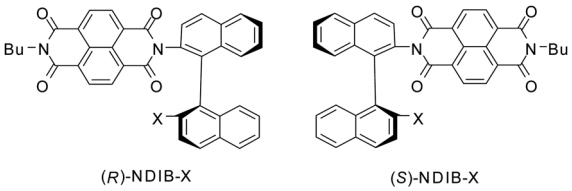

Scheme 1 *N*-Butyl naphthalenediimide enantiomers, X = NH_2, $NHCH_3$, OH, OCH_3, NO_2.

coefficients were used. The degree of circularity, DOC, depends on the molecular polarisability.[1–3]

In this study we investigated how the ECD-Raman spectra differed across a series of binaphthyl derivatives, and how the spectra could be related to the molecular structure. We have already reported on the ROA spectra of atropisomeric binaphthalenylamine of *N*-butyl naphthalenediimide NDIB–X, (X = NH_2, Scheme 1).[8] An NDI core has universal properties for building low molecular weight organic semiconductors with: electron (n), hole (p), or ambipolar (n and p) semiconductivity.[20] NDIs exhibit electroluminescence and photoluminescence, as well as photovoltaic and field effects. They have low density and are solution-processable. In addition, elastic surfaces can be covered with NDIs using zone casting, epitaxial growth, or printing.

Furthermore, chiral NDIs are excellent for constructing enantioselective biomedical sensors.[21] The first NDI functionalized voltammetric sensors were developed with our co-operation to selectively determine (*S*)- or (*R*)-thalidomide in blood plasma without the enantiomer separation.[21]

The position of the longest wavelength (first) ECD band of (*S*)-NDIB–NH_2 is solvent-dependent (475–545 nm) and has a negative sign.[8] NDIB–NH_2 is soluble in polar and apolar, small and bulky, slightly proton-donating and proton-accepting solvents, but not in water or alcohols. The first band is due to the HOMO → LUMO transition from electron-rich aminonaphthalene (N–NH_2) to an electron-poor, NDI moiety.[8,20,21] The close vicinity of the NDI and N–NH_2 enables their strong intramolecular electron donor–acceptor (EDA) interaction stabilising the molecule with an extra 17 kcal mol^{-1}.[8]

In this study, we synthesised both enantiomers of NDIB–X, X = OH, $NHCH_3$, OCH_3, and NO_2 (ESI,† synthesis) and for the latter three, we determined the X-ray structures (Fig. 1 and Fig. S1–S7, Table S1, ESI†). The ECD-Raman spectra of the NDIB–X varied with the ECD spectra which varied with the substituent. The main ECD-Raman change came from the shift of the HOMO → LUMO ECD band at 532 nm. For some substituents, the solvent governed the ECD-Raman effect. Unlike in ref. 2, the RROA signals remained unmeasurable.

The exchange of the NH_2 group modified the HOMO state (Tables S2 and S3, ESI†) and the electronic wavelengths (Fig. 2 and Fig. S8–S11, ESI†). In NDIB–X, NDI is the most electron-deficient and LUMO is always located at NDI (Table S3, ESI†). HOMO remains at the linking naphthalene only for the π-electron acceptor groups. The substituent orientation affects the NDIB–X torsion angles that are important for the HOMO localization and the ECD sign (Table S3 and Fig. S12–S15, ESI†).

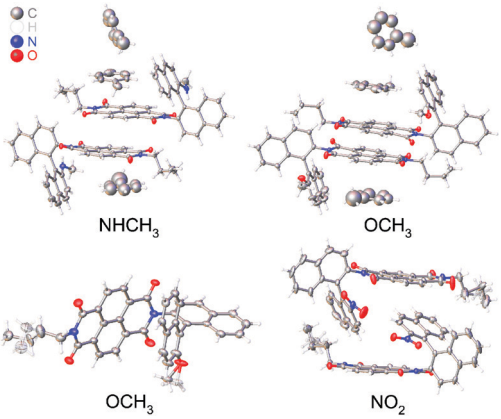

Fig. 1 X-Ray structures of NDIB–X, X = $NHCH_3$, OCH_3, and NO_2. The $NHCH_3$ and OCH_3 derivatives crystallised from toluene (top) had the solvent in the crystal cell.

In the experiment, the change of these torsion angles could be induced by a solvent. In fact, the ECD sign of the (*S*)-NDIB–OH first band was negative for the $CHCl_3$ or C_6H_5CN, but positive for the proton-accepting DMSO, pyridine, and dimethyl acetamide (DMA) solvents (Fig. 2 and Fig. S11, ESI†). In general, the shape and the localization of HOMO depended on: (i) the

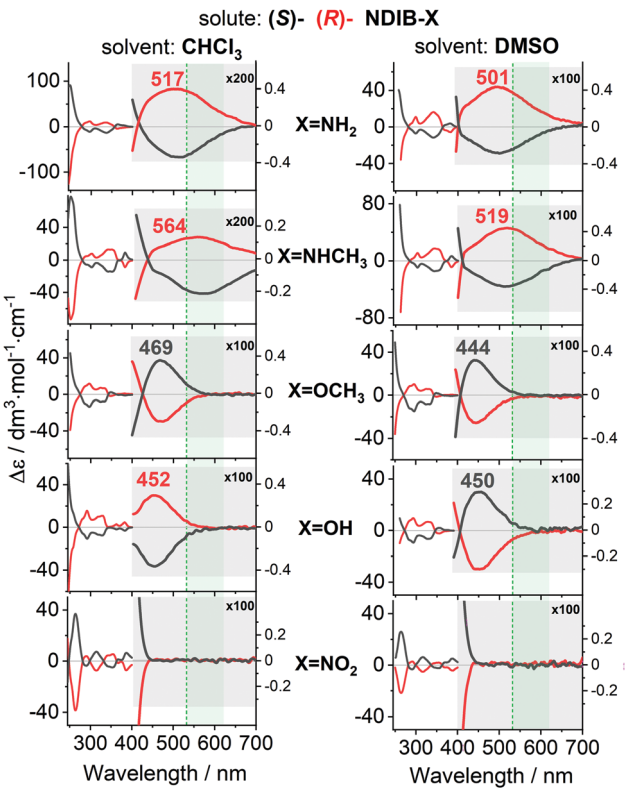

Fig. 2 ECD spectra of (*R*/*S*)-NDIB–X for various substituents and solvents. The green, dotted line and the green range indicate the 532 nm laser excitation, and the detected scattering range (532–610 nm) in the ROA/Raman experiment respectively. The 532–610 nm range corresponds to the approximately 0–2400 cm^{-1} spectral range in the Raman shift. The intensity of the longest wavelength ECD band of (*R*/*S*)-NDIB–X's is magnified 100 or 200 times and is presented in the grey boxes for clarity.

substituent π-electron donor–acceptor ability, and (ii) the molecular conformation/flexibility. The strong π-electron-donating NH_2 and $NHCH_3$ groups[22] stabilised HOMO at the substituted naphthalene moiety (Tables S2 and S3, ESI†), and the first ECD band was near 500 nm (Fig. 2). For the weaker π-electron donors, like OH and OCH_3, the band shifted to *ca.* 450 nm, while the π-electron-accepting groups, like NO_2, caused the relocation of HOMO to the linking naphthalene moiety and the first (HOMO → LUMO) transition was shifted to even lower wavelengths (Fig. 2 and Fig. S9–S11, ESI†). The energy shift was correlated with the amount of the π-electron charge supplied by the substituent to the naphthalene system (Fig. S8 and Tables S2, S3, ESI†).

However, the sign did not change with the solvent for the NH_2 and $NHCH_3$ groups. For the OH there was a sign flip (Fig. 2 and Fig. S12, S14, S15, ESI†). The NDIB–OCH_3 in the $CHCl_3$ had a sign opposite that for the NH_2 and $NHCH_3$. This was related to the direction of the OCH_3 group methyl towards the bulk solvent, irrespective of the solvent proton donor–acceptor properties (Fig. S13, ESI†). The calculations also indicated that the size of the substituent mattered. For example, the $N(CH_3)_2$ group, which is a stronger π-electron donor than the NH_2 and $NHCH_3$,[22,23] did not shift the band towards longer wavelengths than the $NHCH_3$ did (Tables S2 and S3, ESI†).

The ECD-Raman spectra predicted based on eqn (1)[1–3] were concordant with the experimental spectra (Fig. 3, 4 and Fig. S17–S19, ESI†). For all of the systems except for NDIB–NO_2, the intense $CHCl_3$ solvent bands were present, and except for NDIB–NH_2 and NDIB–$NHCH_3$ the solute bands were weak and hidden in the noise. Furthermore, the OCH_3 derivative had a different sign than the others (Fig. 3).

In the DMSO, the spectra of all of the derivatives followed the changes of the first ECD band and seemed to be monosigned. The OH and OCH_3 derivatives, exhibited the opposite signs to that of the NH_2 and $NHCH_3$ derivatives (Fig. 4). However, the simulations indicated, that for the NDIB–OH and NDIB–OCH_3, some bands could have the opposite sign but were too weak to be observed (Fig. 3 and 4). The weak solute bands had the same sign as the solvent, which suggested that they had the ECD-Raman origin as well, and they were weak because of the low solute concentration (*cf.* eqn (1)). Moreover, the intensity of the solute and the solvent bands increased with the solute concentration as predicted by eqn (1) (Fig. S16, ESI†). The DFT computations indicated that if the (true, natural) RROA bands of the solute were present, they should have had the sign opposite that of the ECD-Raman bands (Fig. S20–S29, ESI†). A similar situation was noticed for the transition metal complexes.[1,11,24] Furthermore, one could expect that the possible RROA signal was not due to the resonance with the low-intensity CT transition, but with the more pronounced ECD bands located at *ca.* 400 nm. However, the same sign of the calculated and experimental ROA band could only be obtained at much lower excitation wavelengths, closer to the second electronic transition with the sign of the ECD band opposite to the first transition one (Fig. S20–S29, ESI†). In contrast, for the vitamin B_{12} derivatives, a superposition of the ECD-Raman and

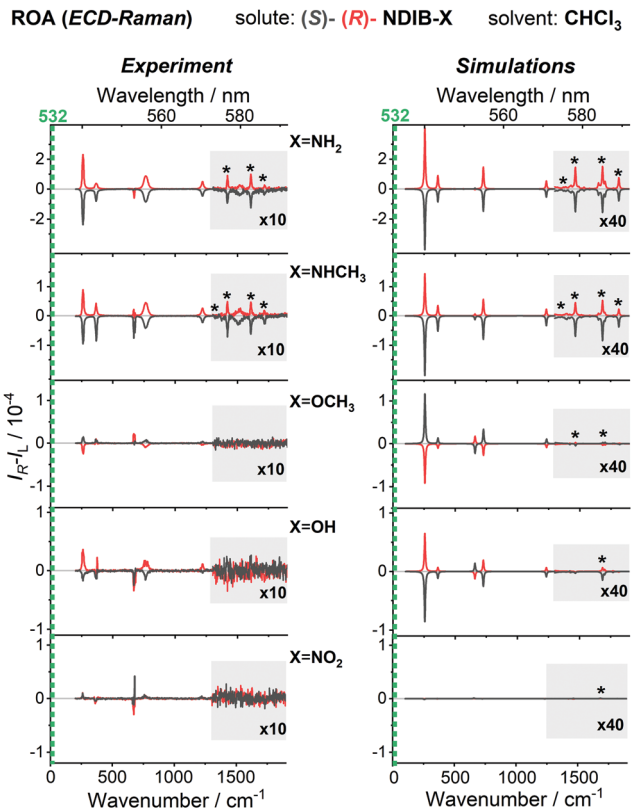

Fig. 3 The effect of the functional groups on the experimental (left) and simulated (right) ECD-Raman spectra of the NDIB–X derivatives. The intensity of the solute bands is magnified 10 or 40 times and is presented in the grey boxes and marked by asterisks.

RROA effects was observed because the change of the concentration or the pathlength allowed the ECD-Raman and RROA signals to be distinguished.[2] Weak RROA was also seen for a vanadium complex, but only after subtraction of the strong ECD-Raman solvent bands.[24] Thus, the RROA bands could be detected/filtrated from the strong ECD-Raman spectra when the strong ECD bands satisfied the resonance condition.[2,24] The NDIB–X ECD bands in resonance were weak which disfavoured the presence of the RROA bands. Although the ECD-Raman signal reflected the electronic properties of the studied compounds well, simultaneous measurement of the natural RROA was still desirable.

For the case of the NDIB–X molecules, we were able to control the ECD-Raman spectra of the solvent by shifting the NDIB–X first ECD band by changing the π-electron activity of the X substituents. The strong π-electron donors located the band near 530 nm while the strong π-electron acceptors shifted the band below 450 nm, *i.e.*, off the resonance. Thus, the ECD-Raman bands of the solvent changed intensities or even signs in a manner that was predictable with eqn (1).

The sign flip of the first ECD band of the NDIB–OH with the change of the solvent (inert *vs.* proton-accepting) suggested that it could be possible to prepare a system with equal concentrations of the intramolecularly and intermolecularly bound solutes. Then, both of the first ECD bands would have opposite signs and could disappear as a result of mutual compensation,

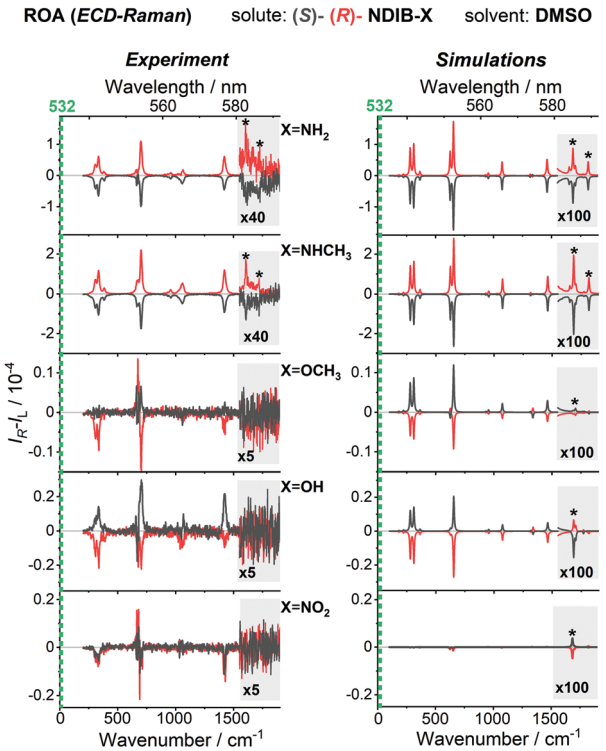

Fig. 4 Experimental (left) and simulated (right) ECD-Raman spectra of NDIB–X derivatives (as shown in Fig. 3) for the DMSO solvent. The intensity of the solute bands is magnified 5, 40 or 100 times and is presented in the grey boxes and marked by asterisks.

while the other ECD bands could still be observed, as well as, the first UV-vis bands. In this type of system, light absorbed by the two forms of solute would not be circularly polarised and the ECD-Raman spectra of the achiral solvent would vanish. For the same reasons, the solute RROA signals could be mutually compensated for. However, the ordinary resonance Raman effect of the solute and ROA spectra of a chiral solute should have been observed.

In conclusion, the ROA measurements performed on chiral molecules absorbed in the Raman scattering range revealed the ECD-Raman signals (polarised Raman scattering modulated by electronic circular dichroism) that dominated the natural Raman optical activity signals. This effect was correctly recognized only in late 2020.[1] For a series of atropisomeric naphthalenediimides, we showed that the ECD-Raman spectra measured with the ROA apparatus were largely dependent on the solute substitution and/or solvent change. The series was the first consistent set of organic compounds exhibiting the ECD-Raman effect. The spectra were well predicted by theory.[1–3,25]

The effect can be observed for any chiral molecule (bearing a chirality centre[1–3] or a chirality axis[8]) exhibiting an ECD band providing (pre)resonance conditions for the incident laser beam light. The ECD-Raman spectrum can show a non-obvious pattern of achiral solvent bands (bisignate or monosignate but negative) with the apparent absence of bands of the chiral solute. In such a case, a distinct ECD-Raman pattern of an achiral solvent can be predicted by the theory[1–3] and can indirectly confirm the presence of the chiral solute in the specific enantiomeric form, and provide an additional tool for monitoring the presence of chiral molecules. Due to the resonance, the ECD-Raman spectral response could be much enhanced in comparison to common ROA spectra, and the signal specificity could be much enhanced in comparison to ECD ones.

All authors participated in writing of the original draft. E. M. investigated the ECD, Raman, and ECD-Raman spectra using ROA spectrometer. G. Z. performed formal analysis of the ECD-Raman spectra and performed some quantum chemical calculations. M. B. conceptualized and developed methodology of all spectroscopic measurements. P. B. conceptualized and developed methodology of interpretation and simulation of the ECD-Raman spectra. D. K. performed NDIB–X syntheses according to methodology and supervision of R. K. K. L. performed X-ray crystallography investigations. J. E. R. realized quantum chemical calculations of ECD, Raman, ROA spectra, and of the solvent effect. J. Cz. D. investigated the substituent effect using DFT calculations, conceptualized and administrated the project.

This work was supported by the National Science Centre in Poland Grants No. 2020/39/B/ST4/01670 to J. Cz. D. and 2019/33/N/ST4/01986 to E. M., and by the Grant agency (20-10144S) and Ministry of Education (CZ.02.1.01/0.0/0.0/16019/0000729) of the Czech Republic to P. B. The computational Grant to J. Cz. D. team from the Świerk Computing Centre (CIŚ) is acknowledged. This research was supported in part by PL-Grid Infrastructure. The project is co-financed by the Polish National Agency for Academic Exchange (No. PPN/BCZ/2019/1/00058/U/00001).

Conflicts of interest

There are no conflicts to declare.

Notes and references

1 T. Wu, *et al.*, *Angew. Chem., Int. Ed.*, 2020, **59**, 21789.
2 E. Machalska, *et al.*, *Angew. Chem., Int. Ed.*, 2021, **60**, 21205–21210.
3 G. Li, *et al.*, *Angew. Chem., Int. Ed.*, 2021, **60**, 22004–22009.
4 L. A. Nafie, *Chirality*, 2020, **32**, 667–692.
5 M. Krupová, J. Kessler and P. Bouř, *ChemPlusChem*, 2020, **85**, 561–575.
6 J. Šebestík, F. Teplý, I. Císařová, J. Vávra, D. Koval and P. Bouř, *Chem. Commun.*, 2016, **52**, 6257–6260.
7 G. Li, *et al.*, *Angew. Chem., Int. Ed.*, 2019, **58**, 16495–16498.
8 E. Machalska, *et al.*, *Chem. Sci.*, 2021, **12**, 911–916.
9 L. A. Nafie, *Chem. Phys.*, 1996, **205**, 309–322.
10 M. Vargek, *et al.*, *Chem. Phys. Lett.*, 1998, **287**, 359–364.
11 C. Merten, H. Li and L. A. Nafie, *J. Phys. Chem. A*, 2012, **116**, 7329–7336.
12 L. Jensen, *et al.*, *J. Chem. Phys.*, 2007, **127**, 134101.
13 S. Luber, J. Neugebauer and M. Reiher, *J. Chem. Phys.*, 2010, 132.
14 J. Mattiat and S. Luber, *J. Chem. Phys.*, 2019, **151**, 234110.
15 G. Zajac, *et al.*, *J. Raman Spectrosc.*, 2014, **45**, 859–862.
16 G. Zajac, *et al.*, *J. Phys. Chem. B*, 2015, **119**, 12193–12201.
17 G. Zając and P. Bouř, *J. Phys. Chem. B*, 2022, **126**, 355–367.
18 G. A. Jones and D. S. Bradshaw, *Front. Phys.*, 2019, **7**, 100.
19 R. Clark, *et al.*, *J. Am. Chem. Soc.*, 1974, **96**, 5586–5588.
20 S. V. Bhosale, M. Al Kobaisi, R. W. Jadhav, P. P. Morajkar, L. A. Jones and S. George, *Chem. Soc. Rev.*, 2021, **50**, 9845–9998.
21 A. Kowalczyk, *et al.*, *Biosens. Bioelectron.*, 2020, **167**, 112446.
22 W. P. Oziminski and J. Cz. Dobrowolski, *J. Phys. Org. Chem.*, 2009, **22**, 769–778.
23 J. Cz. Dobrowolski, P. F. J. Lipiński and G. Karpińska, *J. Phys. Chem. A*, 2018, **122**, 4609–4621.
24 E. Machalska, *et al.*, *Phys. Chem. Chem. Phys.*, 2021, **23**, 23336–23340.
25 G. Li, M. Alshalalfeh, J. Kapitán, P. Bouř and Y. Xu, *Chem. – Eur. J.*, 2022, e202104302.